

Zero-Conductance Resonances due to Flux States in Nanographite Ribbon Junctions

Katsunori Wakabayashi^{1,2} and Manfred Sigrist¹

¹*Yukawa Institute for Theoretical Physics, Kyoto University, Kyoto 606-8502, Japan*

²*Institute of Materials Science, University of Tsukuba, Tsukuba 305-8573, Japan*

(Received 15 July 1999)

Electronic transport properties through junctions in nanographite ribbons are investigated using the Landauer approach. In the low-energy regime ribbons with zigzag boundary have a single conducting channel of edge states. The conductance as a function of the chemical potential shows a rich structure with sharp dips of zero conductance. Each zero-conductance resonance is connected with a resonant state which can be interpreted as the superposition of two degenerate flux states with Kekulé-like current patterns. These zero-conductance dips are connected with a pronounced negative magnetoresistance.

PACS numbers: 72.10.-d, 73.23.Ad, 73.40.Rw, 73.50.-h

The discovery of fullerene molecules and carbon nanotubes has triggered intensive research on various nanometer-size carbon materials [1,2]. In these systems, the geometry of sp^2 carbon networks crucially affects the electronic states near the Fermi level. Studies with scanning tunneling microscopy and spectroscopy have confirmed the connection between the electronic states of the single wall carbon nanotubes (SWCN) and their geometry [3]. Recently, the electrical transport measurement of individual SWCN became possible [4–7] and the quantized conductance of multiwall carbon nanotubes was observed [8]. This initiated theoretical studies devoted to effects of nonmagnetic impurities [9], electron correlation [10], and topological defects [11–15]. Besides these closed carbon molecules, there are also systems with open boundaries which display unusual features connected with their shape. They include small scale systems based on graphite, so-called nanographites. There are two basic shapes of regular graphite edges, called armchair and zigzag edges, depending on the cutting direction of the graphite sheet. Properties originating from such edges have been studied recently using the model of graphite ribbons, one-dimensional graphite stripes of infinite length and finite width. Ribbons with zigzag edges (zigzag ribbons) possess electron states localized near the edge with energies very close to the Fermi level [16–18]. Such states are absent for ribbons with armchair edges. The edge states of zigzag ribbons were analyzed in terms of nearest-neighbor tight binding models [16–18] and density functional approach [19]. It was also pointed out that the edge states play important roles in the magnetic properties in nanometer-size systems due to their relatively large contribution to the density of states at the Fermi energy [16,18]. Recently, experimental evidence for edge states has been reported for nanographite systems derived from graphitized diamond nanoparticles [20].

In this Letter, we investigate the transport properties of ribbons related to these edge states. For this purpose we design three different types of junctions which connect zigzag ribbons of the same or different widths. The electronic states are described by a single-orbital nearest-

neighbor tight binding model. The conductance of the junctions is evaluated using the multichannel Landauer formula [21],

$$G(E) = \frac{e^2}{\pi \hbar} \sum_{\mu, \nu} |t_{\mu\nu}(E)|^2, \quad (1)$$

where $t_{\mu\nu}(E)$ is a transmission coefficient from μ th channel to ν th channel at energy E , calculated by a recursive Green's function method [22]. Before discussing the design of the junctions and their conductance properties, we review a few facts concerning the low-energy states in two kinds of graphite ribbons, the zigzag and the “bearded” ribbon (a variant of a zigzag ribbon).

Zigzag ribbon.—The zigzag ribbons are metallic for arbitrary ribbon width. The most remarkable feature is the presence of a partly flat band at the Fermi level, where the electrons are strongly localized near the zigzag edge. Each edge state has a nonvanishing amplitude only on one of the two sublattices, i.e., nonbonding character. However, in a zigzag ribbon of finite width, two edge states coming from both sides have finite overlap. Because they are located on different sublattices, they mix into a bonding and antibonding configuration. In this way the partly flat bands acquire a dispersion [Fig. 1(b)]. Note that the overlap is increasing as k deviates from π/a , because the penetration depth of the edge states increases and diverges at $k = 2\pi/3a$, where a is the lattice constant. The dispersion depends on the ribbon width N (number of zigzag lines from one side to the other). Close to $k = \pi/a$, the spectrum has the approximate form $E_k = \pm 2tND_k^{N-1}(1 - D_k/2)$, where $D_k = 2\cos(\frac{ka}{2})$, and t is the hopping matrix element. Thus, although the edge states on each side separately have nonbonding character, together through their overlap they provide one conducting channel except at exactly $E = 0$. The energy region of single-channel transport is restricted by the energy gap (Δ_z) to the next channel $\Delta_z = 4t\cos[(N-1)\pi/(2N+1)]$ [18].

Bearded ribbon.—The bearded ribbon has one zigzag edge and one edge which has additional bonds (beard) attached to the zigzag edge [Fig. 1(a), region M]. The edge

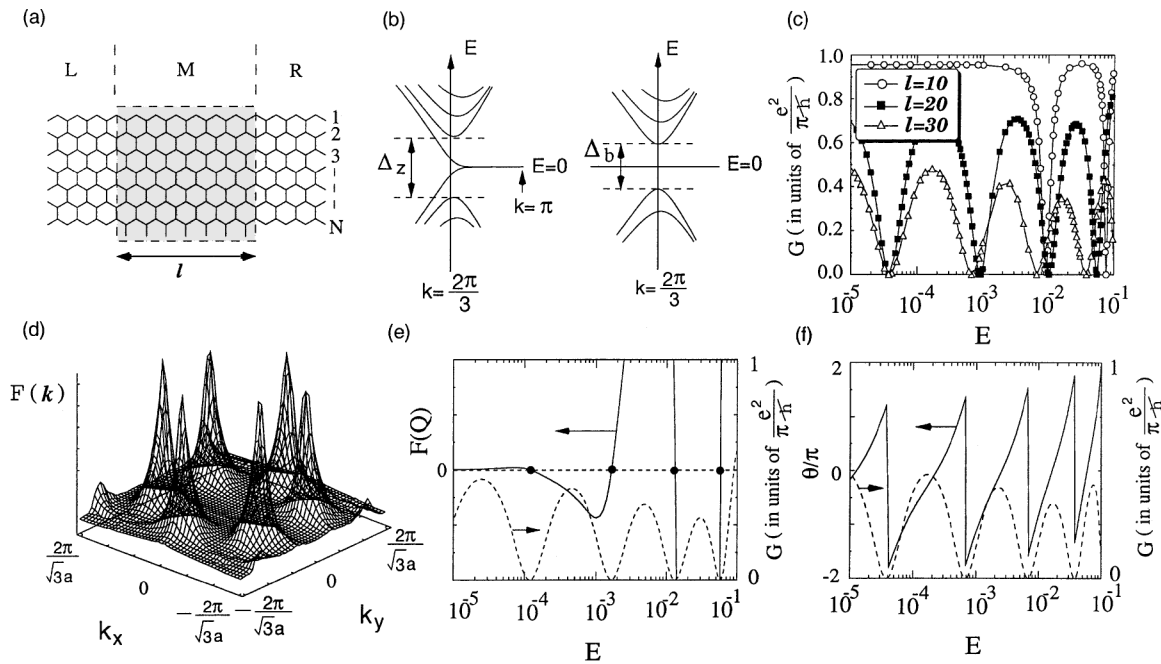


FIG. 1. (a) The structure of the graphite ribbon junction. The length of the junction, l , is given by the number of attached bonds in the shaded region. (b) The schematic figure of energy band dispersion near $E = 0$ of zigzag ribbons (left) and bearded ribbons (right). (c) The energy dependence of the conductance, for $l = 5, 10, 15$, and $N = 30$. (d) The Fourier transform $F(\mathbf{k})$ shows a dominant peak structure corresponding to the Kekulé-like circular current pattern. (e) The energy dependence of the peak value $F(\mathbf{Q})$ showing zeros at the zero-conductance dips. (f) The energy dependence of the phase θ of the transmission coefficient of $l = 15$ when $N = 30$ (dashed line shows the conductance).

states of both sides reside on the same sublattice so that in spite of their overlap their nonbonding character is retained and a completely flat band at $E = 0$ is resulting for any width N [Fig. 1(b)]. The absence of dispersion leads to the insulating behavior for the edge state channel. The gap (Δ_b) to the first conducting channel is given by $\Delta_b = 4t \cos[N\pi/(2N + 2)]$ [18].

We now turn to the design of a junction connecting two zigzag ribbons denoted by L (left) and R (right). As a first example, we consider the case depicted in Fig. 1(a) where the junction region denoted by M is a bearded ribbon of length l (number of attached bonds). This junction model represents a metal-insulator-metal junction providing an illustrative example for the peculiar transport properties of graphite ribbons regardless of the question as to whether bearded ribbons could be realized in nature. We calculate the conductance $G(E)$ numerically within the energy range $|E| < \Delta_b/2$. The result for $N = 30$ and different values of l is shown in Fig. 1(c) using a logarithmic scale on the energy axis. The most striking feature is the large number of zero-conductance dips at energy values which depend on l . These dips represent resonances of total reflection. In the whole energy range no transmission resonances are observed for any value of l . Note also that the change of N does not lead to a qualitative change and only modifies the energy range of single-channel conductance.

Resonances are associated with discrete quantum levels in the junction regions. In the following we would like to

characterize the quantum states encountered here and discuss the origin of total reflection. It was noticed earlier that some graphite ribbons form a triangular Kekulé pattern of circular current driven by special external boundary conditions [18]. To investigate whether the junction states responsible for the resonance display a similar structure, we introduce the current vortex amplitude defined on the dual (triangular) lattice as the clockwise circular sum of the currents $I_{i,p}$ on the bonds of the p th hexagonal plaquette, $V_p = \sum_{i=1}^6 I_{i,p}$. An incident current from the left lead L yields a flow in the junction region. The pattern of V_p is most easily visualized by its Fourier transform, $F(\mathbf{k}) = \sum_p V_p \cos(\mathbf{k} \cdot \mathbf{r}_p)$ in the junction region [\mathbf{r}_p : coordinate of the ring center and $k_x(k_y)$ discrete wave numbers along (perpendicular to) zigzag lines in the junction]. The function $F(\mathbf{k})$ shows a clear peak structure which is dominated by a correlation at finite momenta ($\mathbf{k} = \mathbf{Q}$) as shown in Fig. 1(d) for the case of $l = 15$ and $N = 30$. This corresponds to the anticipated triangular Kekulé current pattern, analogous to a flux state in the sense that a strong correlation among the circular currents exists in the junction. Note that this type of current correlation is present only in the junction region and does not appear in the leads far away from the scattering centers. The correlation peaks $F(\mathbf{Q})$ disappear and change sign at each of the zero-conductance dips [see Fig. 1(e)] as well as $F(\mathbf{k} = 0)$ which represents the overall vorticity of the current flow [28]. Also the average $\langle |V_p| \rangle$ vanishes at the zero-conductance

dip, confirming clearly that no circular current is flowing in every individual plaquette. These properties show that the resonant state leading to the total reflection can be understood as a standing wave resulting from the superposition of a triangular Kekulé current pattern of opposite chirality.

The presence of this quantum level plays an important role for the realization of the zero-conductance resonances. At each resonance the transmission is not only carried by the usual tunneling through the insulating junction region, but also through this resonant state. This decomposition into two channels can yield the following form for the transmission amplitude between the two leads close to a resonance at energy E_0 :

$$\begin{aligned} t(E) &= \tilde{t}(E) \left(1 - \frac{i\Gamma/2}{E - E_0 + i\Gamma/2} \right) \\ &= \frac{\tilde{t}(E)(E - E_0)}{E - E_0 + i\Gamma/2}, \end{aligned} \quad (2)$$

where $\tilde{t}(E)$ is a regular complex function of E and Γ the width of the resonance. The destructive interference of the two channels is a consequence of the symmetric form of the S matrix which relates the in- and outgoing waves of the two leads with those of the junction region [23]. This situation has been discussed in the context of the three-way splitter and a rigorous proof was given for the exact canceling at the resonant energies [23]. A consequence of this resonant form of the transmission amplitude [Eq. (2)] is that the phase θ of $t(E)$ exhibits a jump by π at each resonance; see Fig. 1(f) (similar to Refs. [24,25]). The behavior of the phase is well described by Eq. (2). The form of the S matrix mentioned above as well as the degeneracy of the flux states of opposite chirality, combining to a standing wave state, are based on time reversal symmetry. This symmetry can be destroyed by applying a magnetic field. We observe a pronounced negative magnetoresistance at the zero-conductance dip where the conductance grows proportionally to B^2 for small magnetic fields B , as we will discuss in detail elsewhere. We would like to mention here that circular currents associated with zero-conductance dips were recently also reported for two-dimensional wave guides including junctions with stub geometry [26]. Also in this case a negative magnetoresistance should occur.

Next, we discuss two junctions with a more realistic design which do not contain bearded ribbons. They are shown in Fig. 2(a) and connect zigzag ribbon leads of different width (we show $N_L = 50$ and $N_R = 30$ as a representative case). The M region contains a tilted zigzag edge for junction A and an armchair edge for junction B. The conductance of the two junctions is qualitatively different. The tilted edge in A supports an edge state, similar to the bearded ribbon, on the same sublattice as the edge state on the other side. Indeed, we find a very similar behavior of the conductance with a large number

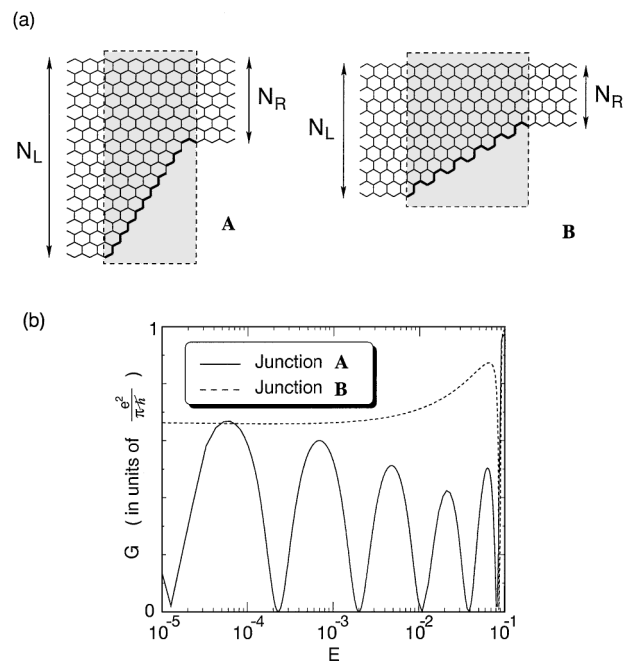


FIG. 2. (a) The structure of graphite ribbons junction type A and type B. (b) The energy dependence of the conductance for $N_L = 50$ and $N_R = 30$.

of zero-conductance resonances [Fig. 2(b)] which are associated with flux states too. For junction B there is no localized state near the armchair edge. The conductance is rather featureless without any resonance in the energy regime of single-channel transport. There is a zero-conductance dip above the single-channel regime of the lead on the left-hand side [$E > \Delta_z(N = 50)/2 = 0.098t$] for both junctions. The origin is also connected with analogous junction states which are based on flux states as the analysis of the current pattern [$F(\mathbf{k})$] shows, although the conditions are different here, since the transmission occurs from three channels on the left-hand side to a single channel on the right-hand side. We omit here a detailed discussion of this more complicated case. For energies above the single-channel threshold of the right-hand side lead [$E > \Delta_z(N = 30)/2 = 0.154t$] no zero-dip features appear in any case.

From this analysis we conclude that the edge structure of the junction plays an important role in forming the resonant states in the M region. It is well known that the electron states display chiral properties in graphite sheets, if there is an imbalance between the two sublattices, e.g., by different onsite potential [27]. The edge states on zigzag edges are a consequence of this imbalance, since the outermost sites belong to a single sublattice. The abrupt change of the sublattice on the edge as it occurs for the previous junction and junction A yields the boundary condition to form the degenerate flux states in the M region. These flux states combine to one resonant state of standing-wave nature. Further numerical analysis shows that even single nonmagnetic impurities and other simple defect structures

disturbing the sublattice balance can cause a zero-conductance dip associated with flux states in zigzag ribbons.

In conclusion, we numerically analyzed three types of nanographite junctions. We found that the conductance of various junctions having zigzag edges shows many zero-conductance dips as a function of energy (chemical potential). These dips are identified as resonances connected with resonant states based on flux states which form circular-current Kekulé patterns. It is obvious that the topology of the edges is crucial for this phenomenon and the chirality connected with the sublattice structure plays an important role. The time reversal symmetry necessary for the existence of these resonances is violated by external magnetic fields, leading to negative magnetoresistance. While the structures used in the calculation might be difficult to produce at present [28], our results also suggest that transport properties of defective carbon nanotubes, carpet-roll, or papier-mâché structures [29] could be rather different from the transport properties of usual closed multiwall nanotubes or SWCN which have only weak features in the low-energy regime [14]. The present study not only clarifies the importance of the edges and their shapes on transport properties, but also indicates the importance of theoretical studies to explicate the interplay between the transport properties and the network topology of carbon atoms. The present numerical work provides the foresight concerning the analysis based on a low-energy effective theory, which is beyond the scope of this paper and will be presented elsewhere. Such an effective theory will serve as a basis for designing carbon-based electronic devices and for further theoretical work on the effects of impurities or electron correlation.

The authors are grateful to T. Enoki, C. Oshima, A. Furusaki, H. Yoshioka, K. Kusakabe, K. Nakada, S. Okada, M. Igami, Y. Takagi, and H. Tsunetsugu for many helpful discussions. This work was supported partly by Grants-in-Aid for Scientific Research No. 10309003 and No. 10640341 from the Ministry of Education, Science and Culture, Japan. K.W. acknowledges the financial support of the Japan Society for the Promotion of Science for Young Scientists. Numerical calculations were performed in part on VPP500 in the Institute for Solid State Physics, University of Tokyo and on SX5 in the Institute for Molecular Science.

- [1] M.S. Dresselhaus, G. Dresselhaus, and P.C. Eklund, *Science of Fullerenes and Carbon Nanotubes* (Academic Press, San Diego, 1996).
- [2] R. Saito, G. Dresselhaus, and M.S. Dresselhaus, *Physical Properties of Carbon Nanotubes* (Imperial College Press, London, 1998).
- [3] J.W.G. Wildöer *et al.*, *Nature (London)* **391**, 59 (1998); T.W. Odom *et al.*, *Nature (London)* **391**, 62 (1998).
- [4] P.L. McEuen *et al.*, cond-mat/9906055; C. Dekker, *Phys. Today* **52**, 22 (1999), for reviews.
- [5] M. Bockrath *et al.*, *Science* **275**, 1922 (1997).
- [6] A. Bezryadin *et al.*, *Phys. Rev. Lett.* **80**, 4036 (1998).
- [7] S.J. Tans *et al.*, *Nature (London)* **386**, 474 (1997).
- [8] S. Frank *et al.*, *Science* **280**, 1744 (1998).
- [9] T. Ando *et al.*, *J. Phys. Soc. Jpn.* **67**, 1704 (1998); **67**, 2857 (1998).
- [10] Y.A. Krotov *et al.*, *Phys. Rev. Lett.* **78**, 4245 (1997); C. Kane *et al.*, *Phys. Rev. Lett.* **79**, 5086 (1997); R. Egger *et al.*, *Phys. Rev. Lett.* **79**, 5082 (1997); H. Yoshioka *et al.*, *Phys. Rev. Lett.* **82**, 374 (1999).
- [11] L. Chico *et al.*, *Phys. Rev. Lett.* **81**, 1278 (1998); **76**, 971 (1996).
- [12] R. Tamura *et al.*, *Phys. Rev. B* **55**, 4991 (1997).
- [13] H. Matsumura *et al.*, *J. Phys. Soc. Jpn.* **67**, 3542 (1998).
- [14] R. Tamura *et al.*, *Phys. Rev. B* **58**, 8120 (1998).
- [15] M. Igami *et al.*, *J. Phys. Soc. Jpn.* **68**, 716 (1999).
- [16] M. Fujita *et al.*, *J. Phys. Soc. Jpn.* **65**, 1920 (1996).
- [17] K. Nakada *et al.*, *Phys. Rev. B* **54**, 17954 (1996).
- [18] K. Wakabayashi *et al.*, *Phys. Rev. B* **59**, 8271 (1999).
- [19] Y. Miyamoto *et al.*, *Phys. Rev. B* **59**, 9858 (1999).
- [20] O.E. Andersson *et al.*, *Phys. Rev. B* **58**, 16387 (1998).
- [21] M. Büttiker *et al.*, *Phys. Rev. B* **31**, 6207 (1985); R. Landauer, *Z. Phys. B* **68**, 217 (1987).
- [22] A. MacKinnon, *Z. Phys. B* **59**, 385 (1985); T. Ando, *Phys. Rev. B* **44**, 8017 (1991).
- [23] Z. Shao *et al.*, *Phys. Rev. B* **49**, 7453 (1994).
- [24] H.-W. Lee, *Phys. Rev. Lett.* **82**, 2358 (1999).
- [25] T. Taniguchi and M. Büttiker, *Phys. Rev. B* **60**, 13814 (1999).
- [26] H. Xu and W. Sheng, *Superlattices Microstruct.* **25**, 79 (1999).
- [27] G.W. Semenoff, *Phys. Rev. Lett.* **53**, 2449 (1984).
- [28] M. Terai *et al.*, *Appl. Surf. Sci.* **130–132**, 876 (1998); C. Oshima (private communication).
- [29] O. Zhou *et al.*, *Nature (London)* **263**, 1744 (1994); S. Amelinckx *et al.*, *Nature (London)* **267**, 1334 (1995).